HHS Public Access

Author manuscript

J Comput Neurosci. Author manuscript; available in PMC 2019 June 27.

Published in final edited form as:

J Comput Neurosci. 2013 April ; 34(2): 211–229. doi:10.1007/s10827-012-0416-6.

Relating ion channel expression, bifurcation structure, and diverse firing patterns in a model of an identified motor neuron

Marco A. Herrera-Valdez[#],
Institute of Interdisciplinary Research, University of Puerto Rico at Cayey, 205 Antonio R. Barcelo Ave., Cayey, PR 00736, USA

Department of Mathematics and Physics, University of Puerto Rico at Cayey, Cayey, PR 00736, USA

Department of Mathematics, University of Arizona, Tucson, AZ 85721, USA

Evelyn F. McKnight Brain Institute, University of Arizona, Tucson, AZ 85724, USA

Erin C. McKiernan[#],
Institute of Interdisciplinary Research, University of Puerto Rico at Cayey, 205 Antonio R. Barcelo Ave., Cayey, PR 00736, USA

Sandra D. Berger,
School of Life Sciences, Arizona State University, Tempe, AZ 85287, USA

Stefanie Ryglewski,
School of Life Sciences, Arizona State University, Tempe, AZ 85287, USA

Johannes Gutenberg University Mainz, Institute for Zoology/Neurobiology, 55099 Mainz, Germany

Carsten Duch, and
School of Life Sciences, Arizona State University, Tempe, AZ 85287, USA

Johannes Gutenberg University Mainz, Institute for Zoology/Neurobiology, 55099 Mainz, Germany

Sharon Crook
School of Mathematical and Statistical Sciences, Arizona State University, Tempe, AZ 85287, USA

[#] These authors contributed equally to this work.

Abstract

Neurons show diverse firing patterns. Even neurons belonging to a single chemical or morphological class, or the same identified neuron, can display different types of electrical activity. For example, motor neuron MN5, which innervates a flight muscle of adult *Drosophila*, can show distinct firing patterns under the same recording conditions. We developed a two-

Erin.McKiernan@upr.edu.

Electronic supplementary material The online version of this article (doi:10.1007/s10827-012-0416-6) contains supplementary material, which is available to authorized users.

dimensional biophysical model and show that a core complement of just two voltage-gated channels is sufficient to generate firing pattern diversity. We propose *Shab* and $DmNa_{\upsilon}$ to be two candidate genes that could encode these core currents, and find that changes in Shab channel expression in the model can reproduce activity resembling the main firing patterns observed in MN5 recordings. We use bifurcation analysis to describe the different transitions between rest and spiking states that result from variations in Shab channel expression, exposing a connection between ion channel expression, bifurcation structure, and firing patterns in models of membrane potential dynamics.

Keywords

Bifurcation; Electrophysiology; Excitability; Firing pattern; Gene expression; Ion channels

1 Introduction

The brain contains a variety of neurons displaying different types of electrical activity (Connors and Gutnick 1990; Tan et al. 2007). Even within neuronal classes, firing patterns are variable. For example, cortical neurons are often classified based on their electrophysiological profiles, which include regular spiking (RS) and fast spiking (FS) (Connors and Gutnick 1990; Steriade 2001). Many FS neurons express γ -aminobutyric acid (GABA) and show a non-pyramidal morphology, while most RS neurons are glutamatergic pyramidal or spiny stellate cells, supporting the idea that neurons of a chemical or morphological class can also be distinguished by their activity (Connors and Gutnick 1990; Steriade 2001). However, under certain stimulation conditions, the same recorded neuron can transition between RS and FS profiles (Steriade et al. 1998).

Variability is also seen in recordings from invertebrate neurons. For example, cultured *Drosophila* embryonic neurons respond to current stimulation with graded peaks, single action potentials (APs), or multiple APs (Peng and Wu 2007; Saito and Wu 1991). Multiple AP firing patterns are further divided into adaptive, tonic, delayed, and damping firing (Peng and Wu 2007). Recordings from flight motor neuron 5 (MN5) in adult *Drosophila* show at least four distinct responses to current stimulation, including single APs, tonic, and delayed firing (Duch et al. 2008). How can the same identified neuron produce such diverse electrical activity?

Neuronal activity is primarily mediated by channels that facilitate transmembrane movement of ions, such as sodium (Na^+) and potassium (K^+) (Hille 2001). Ion channels, particularly those permeable to K^+, are diverse (Coetzee et al. 1999; Jan and Jan 1990; Salkoff et al. 1992). Functional pore-forming (α) subunits of voltage-gated K^+ (Kv) channels are encoded by 4 gene subfamilies: *Kv1* (*Shaker*), *Kv2* (*Shab*), *Kv3* (*Shaw*), and *Kv4* (*Shal*) (Jan and Jan 1997; Salkoff et al. 1992). Kv genes encode channels with distinct voltage sensitivities and kinetics (Coetzee et al. 1999; Salkoff et al. 1992). Diversity is increased by splice variants (Baro et al. 2001; Timpe et al. 1988), heteromultimeric channels (Isacoff et al. 1990), and modulatory beta subunits (Heinemann et al. 1996). Consequently, determining the

contribution of a specific ion channel gene to neuronal excitability is rarely clear-cut experimentally (Trimmer and Rhodes 2004).

Modeling provides a unique opportunity to explore the contribution of specific ionic currents to the variety of firing patterns neurons can display (Günay et al. 2008; Prinz et al. 2003). We developed a two-dimensional biophysical model to simulate membrane potential dynamics of *Drosophila* MN5. The model includes voltage-gated Na^+ and K^+ currents and a leak current. The parameters for the Na^+ and K^+ currents were chosen to represent channels encoded by the $DmNa_v$ (Lin et al. 2009; O'Donnell Olson et al. 2008) and *Shab* (Tsunoda and Salkoff 1995b) genes, respectively. Elimination of Shab currents prevents repetitive firing in *Drosophila* neurons, showing it is a major player in the regulation of neural activity patterns (Peng and Wu 2007). Using the model, we studied the range of firing behaviors produced by varying Shab channel expression. We find that small changes in Shab expression produce the primary firing patterns recorded from MN5, including delayed firing which is thought to require the presence of a transient (A-type) K^+ current encoded by the *Shal* gene (Choi et al. 2004; Ping et al. 2011; Schaefer et al. 2010). Thus, we show that a core complement of just two ion currents is sufficient to produce a wide range of firing behaviors, and further identify two candidate genes, *Shab* and $DmNa_v$, that may encode these core currents. We use bifurcation analysis to describe the qualitatively different transitions between rest and spiking states underlying distinct firing profiles, thereby linking ion channel expression, bifurcation structure, and diversity of firing patterns in a minimal model of an identified motor neuron.

2 Methods

2.1 Electrophysiology

Adult *Drosophila melanogaster* were dissected, as described previously (Duch et al. 2008; Ryglewski and Duch 2009). Recordings were made either from flies with targeted expression of GFP in a subset of motor neurons (C380-GAL4; UAS-mCD8-GFP; Cha-GAL80 (Sanyal et al. 2003), or from control flies (strain w1118). No systematic differences were found between flies with or without GFP expression. Preparations were mounted onto a Zeiss fluorescence microscope (Axio-scope 2FS) and perfused with standard solution (Jan and Jan 1976) composed of (in mM): 128 NaCl, 2 KCl, 1.8 CaCl2, 4 MgCl2, 5 HEPES, and ~35 sucrose adjusted as necessary to a final osmolality of 295 mOsm/kg. pH was adjusted with 1 M NaOH to 7.2. Access to MN5 was achieved by removing the ganglionic sheath surrounding the cell with a 0.5 MΩ-resistance patch pipette filled with 2 % protease diluted in buffer. All chemicals were obtained from Sigma-Aldrich (St. Louis, MO).

MN5 could be identified unambiguously either following expression of UAS-GFP under the control of the motor neuron driver C380-GAL4 (Ryglewski et al. 2012; Sanyal et al. 2003), or by Dye I injection into the target muscle fiber of MN5 12 hours before dissection to allow enough time for retrograde dye diffusion into MN5 somata (for w1118 flies without GFP expression). The Dye I injection technique is described in Ryglewski and Duch (2012).

After cells were exposed and the area washed, MN5 was recorded with a 5.8–6.5 MΩ-resistance patch pipette pulled from borosilicate glass (1.5 mmOD/1 mm ID no filament,

World Precision Instruments) with a Narishige vertical puller. Pipettes were filled with internal solution consisting of (in mM): 140 Kgluconate, 2 MgCl2,11 EGTA, 10 HEPES, 2 MgATP. As needed, pH was adjusted to 7.2 with 1M KOH and osmolality adjusted to 300 mOsm/kg with glucose. Electrical activity of MN5 was recorded *in situ* using somatic patch clamp, as described previously (Duch et al. 2008; Ryglewski and Duch 2009; Ryglewski et al. 2012). Briefly, a gigaseal was first obtained and then negative pressure was applied to enter the whole-cell configuration. Recordings were made at room temperature (~22 °C), amplified with an Axopatch 200B, digitized at 20 kHz with a Digidata 1322A, and stored and analyzed with pCLAMP 10.2 software (all from Molecular Devices). Whole-cell capacitance was 127 ± 16 pF and membrane input resistance was 97 ± 31 MΩ. MN5 was stimulated with square pulse injections of current between 100 pA and 2 nA.

2.2 Neuron model

2.2.1 General expressions for currents—

Channel-mediated currents are the result of electrical drift and diffusion. Since the commonly used conductance-based (CB) model does not incorporate diffusion, we use the electrodiffusion (ED) model formulation derived by Endresen et al. (2000) and later expanded by Herrera-Valdez (2012). The CB model is a linear approximation of the ED formulation, the latter having several advantages over the former, as discussed in detail in Herrera-Valdez (2012). Briefly, experimental data from a variety of neurons show current-voltage (I–V) relationships best fit by a hyperbolic sine (Baranauskas and Martina 2006; Hardie and Minke 1994; Neher 1971), in agreement with the ED derivation. Furthermore, data from current recordings can be directly incorporated into the model without additional calculations of conductance as required by the CB model (Herrera-Valdez 2012).

The whole-cell membrane current carried by a channel permeable to ion *s* has the form

$$I_s = \bar{a}_s p \sinh\left[\frac{z_s}{2v_B}(v - v_s)\right]. \quad (1)$$

The parameter $\bar{a}_s$ represents the maximum amplitude of the current through the open channel (Endresen et al. 2000; Herrera-Valdez 2012) and is a multiple of the number of channels in the membrane. Therefore, $\bar{a}_s$ can be regarded as an indicator of channel expression. The proportion of open channels is represented by p, typically written as a product of gating variables, each taking values between zero and one (Ermentrout and Terman 2010; Izhikevich 2007). A full list of parameters and constants can be found in Table 1.

2.2.2 Membrane potential and specific currents—

The dynamics of the membrane potential can be written as

$$C_m \frac{dv}{dt} = I_S - I_N - I_K - I_L, \quad (2)$$

where I_s, I_N, I_k, and I_L represent, respectively, an externally applied stimulus current, Na^+, K^+, and leak currents. Na^+ channels are modeled after those encoded by the *$DmNa_\upsilon$ (para)* gene expressed in *Drosophila* neurons (Lin et al. 2009; O'Donnell Olson et al. 2008). K^+ channels are based on those encoded by the *shab* gene, the primary contributor to the delayed rectifier current in *Drosophila* muscle and neurons (Tsunoda and Salkoff 1995b). I_L represents currents mediated by electrogenic pumps and channels with relatively small contributions to the change in membrane potential (Chay and Kang 1988; Herrera-Valdez and Lega 2011; Hodgkin and Huxley 1952b; Sonders and Amara 1996).

The currents in the model are:

$$I_K = \bar{a}_K w \sinh\left(\frac{v - v_K}{2v_B}\right), \quad (3)$$

$$I_N = \bar{a}_N m_\infty^3(v)(1 - w) \sinh\left(\frac{v - v_N}{2v_B}\right), \quad (4)$$

$$I_L = \bar{a}_L \sinh\left(\frac{v - v_L}{2v_B}\right). \quad (5)$$

The terms $\bar{a}_K, \bar{a}_N,$ and $\bar{a}_L$ represent the maximal whole-membrane amplitudes of the Shab, $DmNa_\upsilon$, and leak currents, respectively. Activation of K^+ (Shab) channels is represented by the gating variable w as given by:

$$\bar{\tau}_w \frac{dw}{dt} = wB_w^{\sigma_w}(v) - (1 - w)B_w^{\sigma_w - 1}(v), \quad (6)$$

where

$$B_w(v) = B\left(v;\ v_w, \eta_w\right) = \exp\left[\frac{\eta_w}{v_B}\left(v - v_w\right)\right] \quad (7)$$

is a function that describes the steady-state balance between opening and closing rates in the gating mechanism (Endresen et al. 2000). Of note, σ_w specifies the symmetry of the voltage-dependence of the time constant (Herrera-Valdez 2012; Willms et al. 1999) and can be used to control the delay in gating for any change in υ. The steady state of the gate is a function of υ given by

$$w_{\infty}(v) = \left\{1 + 1/B_{w}(v)\right\}^{-1}. \quad (8)$$

Values for the parameters υ_w and η_w were taken directly from data in Tsunoda and Salkoff (1995b), while σ_w was found by modeling the voltage clamp and fitting it to recordings in Tsunoda and Salkoff (1995b) (Online Resource 1). Shab channels inactivate very slowly, so the inactivation variable is assumed to be equal to one (Av-Ron et al. 1993; Connor and Stevens 1971). Activation of Na^+ ($DmNa_\upsilon$) channels m is fast and assumed to be at steady state (Av-Ron et al. 1991; Rinzel 1985), given by an equation of the same form as Eq. (8). The time courses of Na^+ channel inactivation and delayed rectifier K^+ channel activation follow an almost linear relationship (Av-Ron et al. 1991; Rinzel 1985). As a consequence, the inactivation of $DmNa_\upsilon$ channels is approximated by $(1 - w)$ (Av-Ron et al. 1991; Rinzel 1985). Therefore, the state variables of the model are υ and w, as given by Eqs. (2) and (6), respectively. The parameter values used to model each current can be found in Table 1.

2.2.3 Rescaling and parameter estimation—Rescaling of the model and parameter estimation was described in detail previously (Herrera-Valdez 2012). Briefly, all maximum current amplitudes were divided by a normalizing amplitude $\bar{a}$, thereby expressing the amplitudes as ratios of the form $a_s = \bar{a}_s/\bar{a}$. The choice $\bar{a} = \bar{a}_N$ yields

$$a_N = 1,\ a_K = \frac{\bar{a}_K}{\bar{a}_N},\ a_L = \frac{\bar{a}_L}{\bar{a}_N}, \quad (9)$$

and allows investigation, in particular, of the effects of changing the number of K^+ (Shab) channels relative to the number of Na^+ ($DmNa_\upsilon$) channels. As a rule of thumb obtained from analysis herein and previous analyses of the model (Herrera-Valdez 2012), the ratio $a_K = \bar{a}_K/\bar{a}_N$ should be between 1 and 5 when modeling neurons with similar C_m as MN5 and K^+ channels with gating properties similar to those of the Shab channel. Values of $a_K < 1$ typically produce only depolarization block in response to current injection, while $a_K > 5$ tends to produce spiking only with non-physiological levels of injected current and at a frequency exceeding that observed in recordings.

If we let $\xi = \bar{a}_N/C_\mathrm{m}$, Eq. (2) can be written as:

$$\frac{dv}{dt} = \xi\left[J_S - J_N - J_K - J_L\right], \quad (10)$$

where $J = I_s/\bar{a}_\mathrm{N}$. The constant ξ thus acts as a scaling factor to ensure the model produces APs with a dv/dt similar to MN5 recordings. Note that ξ can be adjusted to match experimentally measured dv/dt in other neurons. The value of ξ was set to the average maximum dv/dt from 52 MN5 recordings (~ 100). The average Cm was also taken directly from recordings. Thus, $\bar{a}_n = \xi * C_m$.

The maximum amplitude of the leak current, $\bar{a}_L$, was estimated by taking into account the input resistance, *RIn*, as obtained from MN5 recordings, and calculating $\bar{a}_L \approx 2\upsilon_B/R_{In}$ (Herrera-Valdez 2012). Importantly, although the maximum dv/dt, C_m, and R_{In} did vary some across recordings, our focus was to explore the effects of varying ion channel expression, rather than a change in these parameters. Therefore, a single value, close to the average of each of these measurements as obtained from recordings, was chosen as representative and used for all simulations (see Table 1).

2.2.4 Steady-state current and bifurcation analysis—To assess some of the main computational properties of a model neuron like the one specified in Eqs. (2)–(8), the gating variable w can be replaced by its steady state (i.e. setting $dw/dt = 0$) to obtain the total steady-state current as a function of υ:

$$I_\infty(v) = I_{Na,\infty}(v) + I_{K,\infty}(v) + I_L(v). \quad (11)$$

The system is at steady state if $I_\infty(\upsilon)$ subtracted from the stimulation current I_S equals zero. The set of υ-values that correspond to the fixed points of the system is the set of zeros of $I_S - I_\infty(\upsilon)$, that is $V_* = \{\upsilon_* : I_S - I_\infty(\upsilon) = 0\}$. The monotonicity, or lack thereof, in the curve $I_\infty(\upsilon)$ is an indicator of some of the steady-state bifurcations that can be observed as a function of I_S. Note that $I_S - I_\infty(\upsilon)$ gives the number, but not the type, of fixed points of the system, and it does not help to determine if there are limit cycles.

To study bifurcations due to changes in the type or stability of fixed points, we calculated the two eigenvalues corresponding to each fixed point for different values of I_S. In these kinds of models, and for parameter ranges that overlap with measures from biophysical experiments, the system Eqs. (2)–(8) is expected to have at least one asymptotically stable attractor (Ermentrout and Terman 2010; Izhikevich 2007; Rinzel and Ermentrout 1989). For instance, if all the fixed points are unstable, there is no resting membrane potential and a limit cycle is expected to exist. Since the system is meant to represent a neuron, we set thresholds of 30 mV for the amplitude of oscillations and 10 mV/ms for the maximum dv/dt to detect repetitive spiking. The term *rheobase* is often used in the neuroscience literature to refer to the smallest current required to elicit as few as a single spike with a long (typically 100 s of milliseconds, but theoretically infinite) stimulus of constant amplitude (Fleshman et al. 1981). In our analysis, we are interested in finding the minimum constant stimulus amplitude that triggers repetitive spiking (stable limit cycles). Therefore, we will not use the term rheobase and will instead refer to such a minimum stimulation as *cycle trigger* current, or I_{cyc} in short. Note that using ever-smaller current steps or pulses of longer duration reveals that rheobase is rarely defined as a single unique value (Izhikevich 2007). To address this issue, and keeping in mind a practical connection with experiments, the values of I_{cyc} are reported with a resolution of 1 pA pulse amplitude and 400 ms pulse duration.

2.3 Simulations

All numerical simulations were obtained using Python 2.7 on Lenovo T400 laptops with Intel(R) Core(TM)2 Duo T9600 CPUs at 2.8 GHz running Linux Kubuntu 11. Simulations

were performed using the solver *odeint* contained in the Python module scipy.integrate (Jones et al. 2001), which uses *lsoda* from the Fortran library *odepack*. Depending on the numerics of the simulation, the solver uses Adams' method for nonstiff problems, or a method based on backward differentiation formulas for stiff problems. In addition, *odeint* allows time-step control to test numerical schemes and precision (simulations not shown). The accuracy of the simulations was tested using different time steps and relative tolerances, and it was concluded that the default parameter values for integration give accurate results in an optimal amount of simulation time. The default time step chosen for the time axis of the simulations was 0.025 ms. Figures were produced with the Python module *matplotlib* (Hunter et al. 2008), except for bifurcation diagrams showing the stable and unstable periodic branches, which were generated using XPPAUT (Ermentrout 2006).

3 Results

3.1 MN5 shows distinct firing patterns indicative of different bifurcations of the steady state

MN5 innervates the dorsal longitudinal flight muscle of adult *Drosophila* (Fernandes and Keshishian 1998; Ikeda and Koenig 1988). We recorded from a total of 52 MN5s, 48 (92 %) of which fired in response to current injection. However, not all neurons showed the same firing pattern under the same recording conditions (Fig. 1). Different firing patterns had distinct incidences, and contained features which are consistent with model behaviors that indicate the type of bifurcation producing the transition into or out of spiking.

In response to low-level current injection, 20 of 52 (38 %) MN5s fired a single AP followed by sustained depolarization (Fig. 1(A), black trace). The return to a resting, though depolarized, state is in agreement with a dynamical system that has at least one stable fixed point while current is being injected. This fixed point is probably a node, since the convergence toward rest is not oscillatory (Guckenheimer and Holmes 1990; Izhikevich 2007). The lack of subthreshold oscillations, both transitioning into and out of spiking, is characteristic of a model neuron whose membrane potential is near a saddle-node (SN), rather than an Adronov-Hopf (AH), bifurcation (Guckenheimer and Holmes 1990; Izhikevich 2007). With increasing current, MN5s that previously fired a single AP also fired additional APs with spike frequency adaptation (Fig. 1(A), red trace). Subthreshold oscillations occur prior to the second and third spikes, which is characteristic of systems near an AH bifurcation. However, the initially low firing rate is still suggestive of a SN bifurcation.

In response to low levels of current, 2 of 52 (4 %) of MN5s exhibited repetitive firing, but only after a delay of tens to hundreds of milliseconds (Fig. 1(B), black trace). Although few neurons showed delayed firing, it is interesting to note the presence of this firing pattern in adult motor neurons, since it is one of the prominent patterns in larval motor neurons (Choi et al. 2004; Schaefer et al. 2010). Long delays to first spike are typically observed when the membrane potential of a model neuron is near a SN bifurcation. However, the small and slow oscillation of increasing amplitude prior to the first spike indicates a system that may instead be near an AH bifurcation (Guckenheimer and Holmes 1990; Izhikevich 2007). Alternatively, the subthreshold oscillation could be the result of noise. With larger current,

the firing frequency increased and there was no delay to first spike (Fig. 1(B), red trace). These behaviors do not distinguish between a system transitioning into spiking through either an AH or SN bifurcation, as they could occur in both cases.

Even at low levels of current injection, 22 of 52 (42 %) of MN5s transitioned into spiking very quickly and without a long delay to first spike (Fig. 1(C), black trace). The lack of delay is consistent with a model system that is not near a SN bifurcation (Izhikevich 2007), but this cannot be ruled out since fast spiking can also occur in systems that transition through SN but are stimulated beyond the bifurcation point. A larger current pulse produced faster firing with a negligible decrease in the latency to first spike (Fig. 1(C), red trace), again not leading to a clear prediction about the representative dynamical system.

Finally, 4 of 52 (4 %) showed repetitive firing in response to low current, but with APs that decreased in amplitude and broadened during stimulation (Fig. 1(D), black trace). With more current, the response reduced to a single AP followed by dampening oscillations that ended in depolarization block (Fig. 1(D), red trace). These behaviors correspond to a model membrane whose potential is spiraling towards a stable focus point and thus transitioning *out* of spiking through an AH bifurcation (Guckenheimer and Holmes 1990; Izhikevich 2007).

The differences in the electrophysiological profiles described above indicate topological non-equivalence between the underlying dynamical systems (Izhikevich 2007), and could be due to differences in the levels of ion channel expression. Specifically, we hypothesized that many of the firing profiles observed in MN5 could be generated by changes in the expression of Shab K^+ channels. We focused on Shab channels since they are the primary carrier of delayed rectifier K^+ currents in *Drosophila* neurons (Tsunoda and Salkoff 1995b) and strongly influence repetitive firing (Peng and Wu 2007).

3.2 Shab channel expression is a determinant of the steady-state current-voltage relationship

Shab channel expression is represented in the model by the parameter a_K, which specifies the maximal amplitude of the Shab current relative to the Na^+ ($DmNa_\upsilon$) current. We examined the steady-state current-voltage relationship, $I_\infty(\upsilon)$ in (Eq. 11), for a_K between 1 (equal maximum current amplitudes) and 5 (Shab current amplitude 5 times larger than the $DmNa_\upsilon$ current amplitude). The value of a_K influences both the shape of the steady-state curve as a function of v and the number of zero crossings (Fig. 2). Recall that the zero crossings of $I_\infty(\upsilon)$ occur at the υ-values of the fixed points of the system in the absence of stimulation (vertical dotted line). The curves are non-monotonic with 3 zero crossings for $a_K = 1, 2$ and monotonic with a unique zero crossing for $a_K = 3, 4, 5$. In other words, the number of fixed points decreases from 3 to 1 as the expression of *Shab* increases, thereby producing topologically non-equivalent membranes with potentially different spike-generating mechanisms.

If current is injected ($I_S > 0$), the fixed points are found by examining the crossings at the injected current value (i.e. moving the vertical dotted line in Fig. 2 to the specified I_S). Membranes with different *Shab* expression levels may be topologically equivalent with

respect to the number of fixed points, yet the fixed points may be found at different υ values. Thus, two membranes could display *different* transitions into repetitive spiking for I_S close to that which produces repetitive firing (I_{cyc}), or *similar* spiking behavior for I_S larger than their respective I_{cyc}.

3.3 Shab channel expression is a determinant of the type and stability of fixed points

We analyzed the type and local stability of the fixed points as a function of I_S for a_K in {1, 2, 3, 4, 5} (Fig. 3). Each curve corresponding to a single a_K contains several types of fixed points, indicating that increasing I_S induces sequences of qualitative changes in the behavior of the system. Furthermore, these sequences can differ depending on the value of a_K, even between membranes with the same number of fixed points.

For example, when $a_K = 1$ and I_s is small, the lower branch of the curve up to the knee point includes only stable nodes, while the middle and upper branches contain saddles and unstable foci, respectively (Fig. 3(A), (B), left-most curves). As I_S increases, the number of fixed points decreases from 3 to 1 through a SN bifurcation, leaving an unstable focus as the only fixed point for small I_S and a stable focus for larger I_S. In contrast, when $a_K = 1.4$ or 1.6, the system also has 3 fixed points for small I_S, but the stable nodes in the lower branch become stable foci prior to the SN bifurcation (Fig. 3(B), third and fourth curves from left). Increasing a_K to between 1.8 and 2.4 (Fig. 3(B), fifth through eighth curves from left) causes the stable foci in the lower branch to become unstable, indicating that an AH bifurcation will occur before the SN bifurcation. A neuron with a non-monotonic I_S-υ_* relationship may therefore have an I_{cyc} that does not correspond to the SN bifurcation. This means that $I_\infty(\upsilon)$ cannot always be used as a predictor of the type of transition between rest and repetitive spiking (Izhikevich 2007). Furthermore, although the membranes for a_K between 1 and 2.4 are topologically equivalent, the spike generating mechanisms for select membranes could be different due to the distinct bifurcation sequences.

For $a_K \geq 2.6$, the curves are all monotonic and have the same sequence of changes in the type and stability of the fixed points (Fig. 3(B), last three curves from right). Therefore, these membranes are expected to transition into spiking through the same mechanism. However, the υ-value at which these bifurcations occur is clearly different, with membranes characterized by larger a_K's requiring, for example, more current to produce the transition from stable to unstable foci (i.e. AH bifurcation) in the lower branch. Importantly, as seen previously, an AH bifurcation also occurs for some membranes characterized by a non-monotonic $I-V$ relationship. Therefore, topologically non-equivalent membranes could transition into spiking through the same mechanism.

3.4 Transitions into repetitive spiking vary with Shab channel expression

We characterized the transitions from rest to repetitive spiking for a_K between 1 and 3. The model membrane was stimulated by two 400 ms square pulses, the first 1 pA below I_{cyc} and the second at I_{cyc}. This difference in amplitudes is not meant to reproduce experimental current steps, which often differ by hundreds of pA. Rather, we use this small change in amplitude to see what happens as the membrane moves through the bifurcation. In this reduced system spiking is generated in one of two main ways, depending on the value of a_K.

Interestingly, we expected spiking would be generated by either a SN or AH bifurcation, but instead observed that spiking is produced by either a SN or a fold limit cycle (FLC) bifurcation.

For membranes characterized by $a_K \geq 1.6$, even if topologically non-equivalent, the transition into spiking is through a FLC bifurcation. To illustrate, when $a_K = 2.0$ or 3.0, the membrane responds to current stimulation below I_{cyc} with a single spike early in the pulse (Fig. 4(A1), (B1), black traces). Phase plane analysis shows that for $a_K = 3.0$, the membrane has one fixed point (Fig. 4(A2)), while for $a_K = 2.0$ the membrane has three (Fig. 4(B2)), in the absence of stimulation. In both cases, the fixed point characterizing the resting membrane potential is a stable node. Stimulation converts the node to a focus (Fig. 4(A3), (B3)), but it remains stable, causing the membrane to oscillate back toward a resting (yet depolarized) state for the remainder of the stimulus. As I_S increases to I_{cyc}, repetitive spiking is induced (Fig. 4(A1), (B1), gray traces), but the number and stability of fixed points does not change for either membrane (Fig. 4(A4), (B4)). Repetitive spiking begins when both systems are pushed towards the basin of attraction of a stable limit cycle, which emerges within an I_S window, thus indicating the presence of a bistable regime. (A bifurcation diagram showing the stable and unstable periodic solution branches for the example of a_K = 2.0 can be seen in Online Resource 2.) The emergence (or disappearance) of limit cycles in this way constitutes a FLC bifurcation, and is characteristic of systems near AH bifurcations (Izhikevich 2007). Indeed, for a_K = 2.0 or 3.0, an AH bifurcation occurs when I_S increases beyond I_{cyc}, as seen in the fixed point curves when the focus points in the lower branch lose stability (Fig. 3(B)), but it does not cause the transition into repetitive spiking under this parameter regime.

Repetitive spiking is instead generated by a SN bifurcation in membranes with $a_K \leq 1.4$. For example, when $a_K = 1.2$ or 1.4, current stimulation below I_{cyc} elicits a sustained depolarization of the membrane potential, but no spiking (Fig. 4(C1), (D1), black traces). Both systems have 3 fixed points in the absence of stimulation (Fig. 4(C2), (D2)). Stimulation just below I_{cyc} brings the stable fixed point characterizing the resting potential very close to the saddle point, but three fixed points still remain (Fig. 4(C3)). When I_S increases to I_{cyc}, the two converging points annihilate each other, leaving a single fixed point (Fig. 4(C4)). Thus, both membranes transition into repetitive spiking through a SN bifurcation, producing a long delay to first spike and a subsequently low firing frequency (Fig. 4(C1), gray trace). Note that although only one spike is produced during the 400 ms stimulation period when $a_K = 1.2$, the neuron can be seen to be repetitively spiking if longer current pulses are used (not shown).

The effects of varying a_K within the interval [1,3] on the steady state $I-V$ curve, the bifurcation type, I_{cyc}, delay to first spike, and interspike interval (ISI) associated with the transition into repetitive spiking, are summarized in Table 2.

3.5 Spiking behaviors vary for different combinations of Shab channel expression and current stimulation

To map firing patterns in the model to those seen in MN5, the model membrane was again stimulated with two 400 ms square pulses of current. In these simulations, current

amplitudes were sometimes beyond I_{cyc} and differed by 100 pA to be of the same order of magnitude as current steps used in MN5 recordings. Overall, the results show that certain firing patterns can only be observed for a small range of a_K, while other patterns can be produced over a larger range.

For instance, to observe a profile like that seen in Fig. 1(A), in which small current stimulation produces a single early spike while larger amplitudes elicit repetitive firing, the transition into spiking for this system must be through a FLC bifurcation. The single spike (Fig. 5(A), black trace) is produced when the membrane is pushed away from a stable node, but spirals back towards a stable focus point. Increasing the current by 100 pA pushes the membrane into the basin of attraction for the stable limit cycle and now the neuron spikes repetitively (Fig. 5(A), gray trace). This profile is only observed when $a_K \geq 1.8$. Values below this either cause the membrane to go directly from a graded response (no AP) to repetitive spiking ($a_K = 1.6$; not shown), or to transition through a SN bifurcation, producing late spiking.

One feature of the firing in Fig. 1(A) that we could not reproduce well was spike frequency adaptation. Stimulating single-spiking model neurons with small steps of current just below I_{cyc} produced what is referred to as an adapting or accommodating profile (Mo et al. 2002), in which more than one spike is elicited, but spiking stops prior to the end of the current pulse (Online Resource 3). In some cases, a small decrease in the firing frequency was observed as spiking progressed (e.g. $a_K = 1.8$; Online Resource 3, C1). However, this process was not reproducible for experimentally-realistic current steps and was not due to true adaptation, since adaptation requires at least 3 variables (Guckenheimer et al. 1997).

Reproducing the profile seen in Fig. 1(B), characterized by a long delay (≥~ 100 ms) to first spike at low current amplitudes and tonic firing with no delay at higher amplitudes, requires that the system go through a SN bifurcation. The long delay (Fig. 5(B), black trace) is produced as the trajectory of the system passes close to the region where fixed points were lost in the bifurcation (Izhikevich 2007). When stimulation increases by 100 pA, the delay is no longer present and the firing rate increases (Fig. 5(B), gray trace) as the system traverses a trajectory farther from the aforementioned region. For the parameter regime examined here, the membrane transitions through a SN bifurcation when a_K is between 1.0 and 1.4 (inclusive). Thus, delayed firing is produced only for a small range of a_K. The delayed firing for this regime also differs from that in MN5 in that the firing rate following the delay is arbitrarily low and the ISI is similar in duration to the delay. Delayed firing with an ISI shorter than the delay is achievable with the model, and is addressed in detail in Section 3.6.

The firing profile seen in Fig. 1(C), in which tonic firing commences just after stimulus onset, even in response to low levels of current, can be observed in the model for a large range of a_K. For values of $a_K \geq 1.6$, fast-onset tonic firing is produced at I_{cyc} (i.e. at the FLC bifurcation). If a_K is between 1.0 and 1.4, however, current amplitudes larger than I_{cyc} must be used to push the trajectory away from the region where fixed points were lost during the SN bifurcation (Fig. 5(C)).

The firing profile in Fig. 1(D), in which current stimulation produces broadening spikes and depolarization block at larger amplitudes, can also be seen over a large range of a_K. All values of a_K used herein produce similar triangular-like spikes in response to current stimulation well beyond I_{cyc} (Fig. 5(D), black trace), progressing with dampening oscillations towards depolarization block for larger stimulus amplitudes (Fig. 5(D), gray trace). This transition *out* of spiking is produced as the membrane oscillates back toward a stable focus point.

3.6 Altering channel activation kinetics produces elevated potentials on which spikes ride

Variation in a_K generates the main firing profiles of MN5, but does not reproduce other detailed features of the electrical activity. For example, repetitive spiking in MN5 is characterized by spikes which ride on elevated membrane potentials during current stimulation. Although this feature may result from morphological properties of MN5, such as the structure of the dendritic tree, we were interested in how we could reproduce this aspect of firing in our isopotential model. We predicted that such potentials would be produced by right-shifting the peak of the voltage dependence and adjusting the maximum time constant of Shab activation. This is done by varying the parameters σ_w and $\bar{\tau}_w$, respectively. To stay within the range of experimentally observed variation in Shab current activation (Ryan et al. 2008), we set $\sigma_w = 0.3$, which causes a right-shift in the peak of τ_w relative to υ_w (Willms et al. 1999). To adjust the width of the APs to be ~2.5 ms, we also decreased $\bar{\tau}_w$ to 5 ms. As discussed previously, the model configuration is such that changing the time course of Shab activation also alters DmNa_υ inactivation. Therefore, effects observed under this parameter regime potentially result from changes in the kinetics of both voltage-gated currents.

Simulations and bifurcation analysis were done for a_K between 1 and 5. Under the new parameter regime, the type and stability, but not the location, of the fixed points is changed relative to the previous regime (Online Resource 4). As expected, the altered time course of channel activation produces an elevated membrane potential of ~10–20 mV that persists for the duration of the pulse and on which spikes ride (Fig. 6). Elevated potentials are observed for all a_K in the explored range. Additionally, the spikes are smaller in amplitude and the firing frequency is often higher under this regime (compare to Fig. 5).

We also noticed a type of delayed firing not seen in the previous parameter regime. When $a_K = 1.2$ or 1.4, repetitive spiking is characterized by an ISI smaller than the delay to first spike (Fig. 6(B), (C), black traces). Increasing the current by 100 pA eliminates the long delay and increases the firing frequency (gray traces). Overall, these membrane responses appear more similar to the delayed firing profile observed in MN5 (compare to Fig. 1(B)). The responses differ from MN5 recordings, however, with respect to spike shape. When $a_K = 1.2$, the spikes are concave up during the slow depolarization phase and concave down during the upstroke and repolarization (Fig. 6(C), black trace). This is in contrast to the spikes in the previous parameter regime, which look more like MN5 spikes (compare to Fig. 5). When $a_K = 1.4$, the spike shape improves, but the difference between the delay and the ISI is smaller (Fig. 6(B), black trace). As a_K increases to 2.0, a spike shape resembling that of MN5 is

recovered, but there is no long delay to first spike, and the spike latency and ISI are approximately equal in duration (Fig. 6(A), black trace). Thus, changes in a_K in this regime reveal a trade-off between spike shape and delayed firing.

4 Discussion

One of the current challenges in neurophysiology is to determine what electrical properties are conferred by the wide array of ion channels expressed in neurons. How much redundancy is present? Which currents are necessary or sufficient for producing distinct types of firing? Our results demonstrate that a core complement of just two ion channels may be sufficient to generate the diversity of firing patterns observed in recordings. Since this diversity depends in part on the kinetics of the channels, we further propose that there are a few combinations of channels that are suitable to produce the basic electrophysiological properties of a cell. For MN5, we propose that the core complement of channels could be those encoded by the *Shab* and $DmNa_v$ genes. Furthermore, in our model, the relative maximal amplitudes of the core currents for which the different firing patterns are produced vary no more than one order of magnitude. As a consequence, the model predicts that the range of relative expression between *Shab* and $DmNa_v$ is constrained to a well-defined, and not very large, interval.

4.1 Changes in Shab channel expression produce diverse firing patterns

For this reduced model, small variations in Shab channel expression have profound effects on the transition from rest to repetitive spiking. When Shab channel activation is fast and the density is low, the membrane transitions into spiking through a SN bifurcation, producing long delays to first spike and low initial firing frequencies. In contrast, for the same activation kinetics, increasing Shab channel expression leads to the emergence of a stable limit cycle through a FLC bifurcation, producing a bistable membrane. Current stimulation of sufficient amplitude pushes the membrane into the basin of attraction for the limit cycle, producing repetitive spiking with little to no delay to first spike and fast firing frequencies.

Although experiments to date have not indicated the existence of bistability in MN5, many recorded neurons may not appear to be bistable, even though their membrane is characterized by two stable attractors. The basin of attraction for one of the attractors could be very small, and thus revealing its presence would require a specific combination of initial conditions and small current steps. Furthermore, the fact that hitting upon these conditions is unlikely could cause experimenters occasionally observing this bistability to discard these neurons as ‘unhealthy’, just as some researchers did historically when finding neurons which fire only a single spike (Hodgkin 1948).

It is of particular interest that the model can generate long delays to first spike without a fast inactivating (A-type) current, contrary to the idea that A-type currents, specifically those encoded by *Shal*, are necessary to produce delayed firing in *Drosophila* motor neurons (Choi et al. 2004; Ping et al. 2011; Schaefer et al. 2010). Instead, long delays were produced in the model by setting Shab channel expression low so that the neuron transitions into spiking through a SN bifurcation. Our results do not dispute the involvement of Shal/Kv4-mediated currents in generating delays to first spike; experimental evidence that they play a role in

both *Drosophila* and mammalian (Kim et al. 2005; Shibata et al. 2000) neurons is strong. Rather, we propose that low Shab channel expression is another way in which neurons can produce long delays, potentially compensating for decreased or absent Shal/Kv4-mediated currents. We are not aware of any studies which have demonstrated such a relationship between *Shab* and *Shal* expression, but this prediction is testable by manipulating currents encoded by each gene using a combination of genetic and pharmacological techniques and recording the resulting firing patterns.

4.2 How do variable firing responses in our model relate to MN5 firing patterns as observed during behavior?

MN5 innervates the dorsal longitudinal flight muscle (DLM), which is predominantly used in flight and male courtship song. The DLM is a stretch-activated asynchronous flight muscle, where MN AP are not synchronized with each muscle contraction (Machin and Pringle 1959). Instead, during flight MNs fire single AP at tonic frequencies of 8 to 20 Hz at approximately every 10th to 20th wing beat to fuel the muscle with intracellular Ca^{2+} (Dickinson and Tu 1997). During sustained flight MN1– 5 all fire tonically; they do not show doublets or triplets of spikes and they never fire simultaneously. However, the firing frequencies of all five MNs are modulated simultaneously (Levine and Wyman 1973). The conclusion has been that all flight MNs receive common excitatory drive that is translated into tonic firing at set frequencies (Harcombe and Wyman 1977), which are changed simultaneously in MN1–5 when the power output of the muscle is changed, as during lift (Gordon and Dickinson 2006). Sustained flight thus requires constant tonic MN firing with low spike time precision and slow modulations in firing frequency, depending on power output demands.

In contrast, DLM MNs show different firing patterns during male courtship song. Courtship song is characterized by an initial tone burst with muscle contractions at 160Hz (sine song) during which MNs fire at much lower tonic frequencies than during flight, and some DLM units remain silent (Ewing 1977). Sine song is followed by pulse song, which consists of muscle contraction pulses of 3 ms duration that are separated by interpulse intervals of highly accurate and species-specific durations (34 ms in *Drosophila melanogaster*). Pulse song is characterized by accurately timed MN firing patterns. Consequently, MN5 shows very different firing patterns during flight (tonic firing) and male courtship song (pulse firing). Since both behaviors are thought to share largely similar pre-motor circuitry, MN5 intrinsic properties may contribute to both firing patterns. In fact, ion channel mutations alter pulse song characteristics in *Drosophila* (Schilcher 1976), though it remains unclear whether this is a result of altered MN excitability or of effects elsewhere in the circuit.

Our reduced two-dimensional model indicates that small changes in MN current amplitude and activation kinetics produce qualitatively different transitions between rest and spiking. One possibility may be that during behavior such small changes result from different modulatory states. At least for Drosophila flight, it is known that biogenic amines like octopamine and tyramine have significant effects on take-off likelihood and flight maintenance (Brembs et al. 2007). An important future challenge will be to test whether

different transitions from rest to spiking may result from modulatory input as occurring during normal behaviors such as flight and courtship song.

4.3 Is Shab channel expression a unique solution for producing diverse firing patterns?

Just because our model predicts that changes in Shab channel expression *can* produce an array of firing patterns does not mean that this *is* the way that MN5 (or any other neuron) produces these patterns. Changes in the expression of other ion channels could potentially also do the job. Indeed, experimental work has shown that neurons can generate the same firing pattern with disparate channel expression profiles, demonstrating that there exist functionally equivalent combinations (Schulz et al. 2006).

However, several lines of evidence indicate that changes in Shab channel expression might be a preferred strategy for diversifying firing patterns, as opposed to changes in the expression of other K^+ channels. In *Drosophila*, voltage-gated K^+ channels are encoded primarily by four genes: *Shaker*, *Shal*, *Shaw*, and *Shab* (Salkoff et al. 1992; Tsunoda and Salkoff 1995a). *Shaw*, thought to encode delayed rectifier K^+ currents based on studies in oocytes, was shown in cultured *Drosophila* neurons to instead encode a leak current. Shaw channels have short opening times and very low voltage-sensitivity (Tsunoda and Salkoff 1995b). Thus, *Shaw* would likely make a poor candidate for regulating firing patterns.

Shaker and *Shal* encode voltage-dependent currents, which activate and inactivate rapidly (Ryglewski and Duch 2009; Salkoff et al. 1992). Although they have distinct voltage sensitivities, transient potassium channels encoded by both these genes are maximally active in a voltage range left-shifted relative to Shab channels (Covarrubias et al. 1991; Tsunoda and Salkoff 1995b). Their hyperpolarized voltage sensitivity, in combination with their short open times, mean that Shaker and Shal channels are less likely to be open in the relevant voltage range for generating repetitive firing than Shab channels. It is possible that modeling changes in the expression of Shaker and Shal channels could produce diverse firing patterns, but this would likely require current injection outside the physiological range.

In contrast, variation of *Shab* expression in the model reproduces MN5 firing patterns for values of injected current in agreement with those used in experiments. Experimental work also supports the idea that changes in *Shab* expression can have profound effects on the ability of neurons to produce certain types of repetitive firing (Peng and Wu 2007). Of course, it might be that some of the specific transitions predicted by the model will not be observed, even if the neuron expresses the ‘right’ number of Shab channels. To observe some of these transitions would require that the state of the neuron be very close to the bifurcation point associated with I_{cyc}, and then that the precise amount of current was injected when the neuron was in this state. However, in general, we predict that, neurons expressing low levels of *Shab* would be more likely to display long delays to first spike and low firing frequencies than neurons expressing higher levels of *Shab.*

4.4 Natural variation in channel expression is observed in many types of neurons

In our model, a maximum of a 3 fold change in Shab channel expression reproduced the diversity of MN5 firing behaviors, but is such variation realistic? Research, especially within the last 5–10 years, has demonstrated that neurons show considerable variability in ion

channel expression. In MNs of the crustacean stomatogastric (STG) nervous system, *Shab* mRNA can vary 2–4 fold (Schulz et al. 2006, 2007). In particular, gastric mill neurons show a 4 fold variation in *Shab* mRNA, yet remarkably low levels of *para* (*DmNa*$_v$) expression (Schulz et al. 2007), indicating that the ratio of Shab to DmNa$_v$ channels (a_K) could reach 3 or larger. Variation in channel expression is also seen in other parts of the crustacean nervous system. Large cell MNs within the cardiac ganglion show a more than 3–9 fold variation in mRNA for a variety of ion channels genes, including *Shab*, and as much as a 56 fold variation in *para* mRNA (Tobin et al. 2009).

Similar variation in ion channel expression is observed in mammalian systems. In rats, hippocampal pyramidal cells display a 10 fold variation in the ratio of K^+ to Ca^{2+} mRNA (Eberwine et al. 1992). In mice, dopaminergic neurons within the substantia nigra show a 5–10 fold variation in mRNA encoding for a transient (A-type) potassium channel, and an 8 fold variation in A-type charge density (pC/pF) (Liss et al. 2001). Purkinje neurons in the mouse cerebellum show a 5 fold variation in Na^+ or Ca^{2+} current density (pA/pF) (Swensen and Bean 2005).

Although we are not aware of studies which have measured cell-to-cell variability of *Shab* expression in *Drosophila* MN5, previous work gives us an estimate of the extent to which other K^+ currents vary in this neuron. Recordings from 57 adult *Drosophila* show that total peak transient K^+ current in MN5 can vary nearly 4 fold (Ryglewski and Duch 2009). Furthermore, measures of current densities in embryonic neurons can give us a rough estimate of the ratio of Shab to para/DmNa$_v$ channels (a_K) in the *Drosophila* nervous system. Embryonic MNs show a *Shab-encoded* current density of 60 pA/pF, while *para*-encoded currents are around 30 pA/pF (Baines et al. 2001). Therefore, the estimated a_K is 2, supporting the use in our model of $a_K \geq 1$.

4.5 Changes in Shab activation produce spikes riding on elevated potentials

Altering the rate of Shab current activation by changing the maximum time constant and right-shifting its voltage dependence caused the minimum membrane potential during repetitive spiking to shift up by tens of mVs. Variable activation times have been demonstrated for splice variants of several ion channels (Murbartián et al. 2004; Pan et al. 2001; Saito et al. 1997), and for RNA-edited forms of the Shab channel (Ryan et al. 2008). The rate of K^+ channel activation can also vary due to post-translational mechanisms such as phosphorylation (Schulz et al. 2008), glycosylation (Watanabe et al. 2003), or association with accessory (β) channel subunits (Heinemann et al. 1996; Pongs and Schwarz 2010).

As mentioned previously, it is important to recognize that the formulation of the 2-dimensional model means that a change in the activation kinetics of Shab also changes the inactivation kinetics of DmNa$_v$. Thus, the differences in electrical responses between the two examined parameter regimes could result from a change in the kinetics of both voltage-gated currents. To tease out their relative contributions, future work could include expanding the model to 3 dimensions, where the inactivation of DmNa$_v$ channels is a separate variable. In addition, expansions of the model could include incorporating multiple compartments that would allow us to test how the morphological structure of MN5 contributes to the production of elevated potentials.

4.6 Advantages of the model

A number of minimal models of membrane potential have been proposed previously, but many of these models are not ideal for studying the contribution of ion channel expression to the diversity of firing patterns. For example, the FitzHugh-Nagumo model (Fitz-Hugh 1961; Nagumo et al. 1962), which is a simplification of the classical Hodgkin-Huxley formalism (Hodgkin and Huxley 1952a), is a phenomenological model with equations that do not include terms for channels or channel conductances. The same is true of the later Hindmarsh-Rose model (Hindmarsh and Rose 1984). Although these models are capable of generating different firing patterns, and even bursting in the case of Hindmarsh-Rose, their formulations do not allow one to ask questions about the physiological mechanisms, including differences in ion channel expression, that may produce distinct firing.

Integrate-and-fire models and related formulations using artificial membrane potential resets are computationally inexpensive and can reproduce an impressive diversity of firing patterns seen in cortical neurons (Izhikevich 2003). However, artificial resets at best only capture the dynamics of excitability, but fail to provide biophysical explanations. In contrast, all the parameters in our model can be measured directly from neurons because they have a biophysical correlate. Furthermore, our results relate a measurable parameter, the maximal amplitude of a ionic current encoded by a specific gene, to different firing patterns, thereby offering a biophysical explanation for firing pattern diversity and leading to a number of testable predictions.

Conductance-based (CB) models, based on the standard Hodgkin-Huxley formalism (Hodgkin and Huxley 1952a), are more realistic than the models mentioned above, since they do not include artificial resets, include a number of experimentally measurable parameters, and include channel conductances that can be varied to investigate the role of specific currents. CB models have been used to explore diverse electrical activity in neurons (Arhem and Blomberg 2007; Golomb et al. 2007; Prescott et al. 2008). Arhem and Blomberg (2007) used such a model to relate changes in Na^+ and K^+ channel density to different patterns of repetitive firing, including distinct frequencies and long delays to first spike. Our model is mathematically related to the CB/HH formulation, but incorporates electrodiffusion, which constitutes a theoretical improvement in describing ion movement across the membrane (Endresen et al. 2000; Herrera-Valdez 2012). In addition, while the Arhem and Blomberg model had 4 dimensions, ours was able to reproduce diverse firing behaviors with just 2 dimensions, making it both biophysical and computationally inexpensive.

A 2-dimensional CB/HH model that can reproduce all three of Hodgkin's excitability classes (Hodgkin 1948) was presented by Prescott et al. (2008). Their results showed that varying the half-activation potential of the slow K^+ current was sufficient to convert neuronal firing behavior between the three excitability classes. However, the authors admit that this variation in half-activation is more "drastic" than would likely be seen in a single type of channel. They split the slow current into two separate currents with distinct voltage sensitivities, and hypothesize that these are differentially expressed by neurons displaying different excitability classes. In our model, it was not necessary to vary half-activation or move to 3 dimensions by incorporating additional populations of currents. The slow current

in our model was formulated to represent one type of K^+ current encoded by a single gene (Shab), and differential expression of Shab was sufficient to produce a wide range of firing behaviors.

Importantly, the construction of our model allows extensions to study neurons in other parts of the *Drosophila* nervous system or different developmental stages, as well as neurons in other animals, provided the parameters and core complement of membrane channels are adjusted according to available data from the neurons of interest.

Supplementary Material

Refer to Web version on PubMed Central for supplementary material.

Acknowledgements

MAHV, SDB, SR, CD, and SC were supported in part by the National Science Foundation (NSF IIS 0613404). MAHV and ECM were supported in part by the Building Research Infrastructure and Capacity (BRIC) program at UPR-Cayey (P20 MD006144) through the National Institute of Minority Health and Health Disparities. Support for SDB was also provided by the Interdisciplinary Graduate Program in Neuroscience at Arizona State University. Additional support for SR was provided by the German Research Foundation (DFG RY 117/1-1). We thank Cengiz Gunay, Martin Strube, and Joceline Lega for their challenging and insightful feedback. We also thank two anonymous reviewers whose suggestions greatly improved this paper.

References

Arhem P, & Blomberg C (2007). Ion channel density and threshold dynamics of repetitive firing in a cortical neuron model. Biosystems, 89(1–3), 117–125. [PubMed: 17287076]

Av-Ron E, Parnas H, Segel L (1991). A minimal biophysical model for an excitable and oscillatory neuron. Biological Cybernetics, 65(6), 487–500. [PubMed: 1958734]

Av-Ron E, Parnas H, Segel LA (1993). A basic biophysical model for bursting neurons. Biological Cybernetics, 69, 87–95. [PubMed: 8334193]

Baines R, Uhler J, Thompson A, Sweeney S, Bate M (2001). Altered electrical properties in Drosophila neurons developing without synaptic transmission. Journal of Neuroscience, 21(5), 1523–1531. [PubMed: 11222642]

Baranauskas G, & Martina M (2006). Sodium currents activate without a hodgkin and huxley-type delay in central mammalian neurons. Journal of Neuroscience, 26(2), 671–684. [PubMed: 16407565]

Baro D, Quinones L, Lanning C, Harris-Warrick R, Ruiz M (2001). Alternate splicing of the Shal gene and the origin of I_A diversity among neurons in a dynamic motor network. Neuroscience, 106(2), 419–432. [PubMed: 11566511]

Brembs B, Christiansen F, Pflüger H, Duch C (2007). Flight initiation and maintenance deficits in flies with genetically altered biogenic amine levels. Journal of Neuroscience, 27(41), 11122–11131. [PubMed: 17928454]

Chay T, & Kang H (1988). Role of single-channel stochastic noise on bursting clusters of pancreatic beta-cells. Biophysical Journal, 54(3), 427–435. [PubMed: 2850030]

Choi J, Park D, Griffith L (2004). Electrophysiological and morphological characterization of identified motor neurons in the Drosophila third instar larva central nervous system. Journal of Neurophysiology, 91(5), 2353–2365. [PubMed: 14695352]

Coetzee W, Amarillo Y, Chiu J, Chow A, Lau D, McCormack T, et al. (1999). Molecular diversity of K^+ channels. Annals of New York Academy of Sciences, 868, 233–285.

Connor J, & Stevens C (1971). Inward and delayed outward membrane currents in isolated neural somata under voltage clamp. Journal of Physiology, 213(1), 1–19. [PubMed: 5575338]

Connors B, & Gutnick M (1990). Intrinsic firing patterns of diverse neocortical neurons. Trends in Neurosciences, 13(3), 99–104. [PubMed: 1691879]

Covarrubias M, Wei A, Salkoff L (1991). Shaker, Shal, Shab, and Shaw express independent K-current systems. Neuron, 7(5), 763–773. [PubMed: 1742024]

Dickinson M, & Tu M (1997). The function of dipteran flight muscle. Comparative Biochemistry and Physiology Part A: Physiology, 116(3), 223–238.

Duch C, Vonhoff F, Ryglewski S (2008). Dendrite elongation and dendritic branching are affected separately by different forms of intrinsic motoneuron excitability. Journal of Neurophysiology, 100(5), 2525–2536. [PubMed: 18715893]

Eberwine J, Yeh H, Miyashiro K, Cao Y, Nair S, Finnell R, et al. (1992). Analysis of gene expression in single live neurons. PNAS, 89(7), 3010–3014. [PubMed: 1557406]

Endresen LP, Hall K, Hoye JS, Myrheim J (2000). A theory for the membrane potential of living cells. European Journal of Biophysics, 29, 90–103.

Ermentrout B (2006). PPAUT. Scholarpedia, 2(1), 1399.

Ermentrout G, &Terman D (2010). Mathematical Foundations of Neuroscience. Springer.

Ewing A (1977). The neuromuscular basis of courtship song in Drosophila: the role of the indirect flight muscles. Journal of Comparative Physiology A: Neuroethology, Sensory, Neural, and Behavioral Physiology, 119(3), 249–265.

Fernandes J, & Keshishian H (1998). Nerve-muscle interactions during flight muscle development in Drosophila. Development, 125(9), 1769–1779. [PubMed: 9521914]

Fitz-Hugh R (1961). Impulses and physiological states in theoretical models of nerve membrane. Biophysical Journal, 1, 445–466. [PubMed: 19431309]

Fleshman J, Munson J, Sypert G, Friedman W (1981). Rheobase, input resistance, and motor-unit type in medial gastrocnemius motoneurons in the cat. Journal of Neurophysiology, 46(6), 1326–1338. [PubMed: 6275043]

Golomb D, Donner K, Shacham L, Shlosberg D, Amitai Y, Hansel D (2007). Mechanisms of firing patterns in fast-spiking cortical interneurons. PLoS Computational Biology, 3(8), e156.

Gordon S, & Dickinson M (2006). Role of calcium in the regulation of mechanical power in insect flight. PNAS, 103(11), 4311–4315. [PubMed: 16537527]

Guckenheimer J, Harris-Warrick R, Peck J, Willms A (1997). Bifurcation, bursting, and spike frequency adaptation. Journal of Computational Neuroscience, 4(3), 257–277. [PubMed: 9257235]

Guckenheimer J, & Holmes P (1990). Nonlinear oscillations, dynamical systems, and bifurcations of vector fields. Springer.

Günay C, Edgerton J, Jaeger D (2008). Channel density distributions explain spiking variability in the globus pallidus: a combined physiology and computer simulation database approach. Journal of Neuroscience, 28(30), 7476–7491. [PubMed: 18650326]

Harcombe E, & Wyman R (1977). Output pattern generation by Drosophila flight motoneurons. Journal of Neurophysiology, 40(5), 1066–1077. [PubMed: 409808]

Hardie R, & Minke B (1994). Spontaneous activation of light-sensitive channels in Drosophila photoreceptors. Journal of general physiology, 103(3), 389–407. [PubMed: 8195780]

Heinemann S, Rettig J, Graack H, Pongs O (1996). Functional characterization of Kv channel β-subunits from rat brain. Journal of Physiology, 493(3), 625. [PubMed: 8799886]

Herrera-Valdez M (2012). Membranes with the same ion channel populations but different excitabilities. PLoS ONE, 7(4), e34636.

Herrera-Valdez MA, & Lega J (2011). Reduced models for the pacemaker dynamics of cardiac cells. Journal ofTheoretical Biology, 270(1), 164–176.

Hille B (2001). Ionic channels of excitable membranes (3rd ed.). Sinauer.

Hindmarsh J, & Rose R (1984). A model of neuronal bursting using three coupled first order differential equations. Proceedings of the Royal Society of London. Series B. Biological Sciences, 221(1222), 87–102.

Hodgkin A (1948). The local electric changes associated with repetitive action in a nonmedulated axon. Journal of Physiology, 107, 165–181. [PubMed: 16991796]

Hodgkin A, & Huxley A (1952a). A quantitative description of membrane current and its application to conduction and excitation in nerve. Journal of Physiology, 117, 500–544. [PubMed: 12991237]

Hodgkin A, & Huxley A (1952b). The components of membrane conductance in the giant axon of Loligo. Journal of Physiology, 116(4), 473–496. [PubMed: 14946714]

Hunter J, Dale D, Droettboom M (2008). Matplotlib: a Python 2D plotting library. http://matplotlib.sourceforge.net/.

Ikeda K, & Koenig J (1988). Morphological identification of the motor neurons innervating the dorsal longitudinal flight muscle of Drosophila melanogaster. Journal of Comparative Neurology, 273(3), 436–444. [PubMed: 3145293]

Isacoff E, Jan Y, Jan L, et al. (1990). Evidence for the formation of heteromultimeric potassium channels in xenopus oocytes. Nature, 345(6275), 530–534. [PubMed: 2112229]

Izhikevich E (2007). Dynamical systems in neuroscience. MIT Press.

Izhikevich EM (2003). Simple model of spiking neurons. IEEE Transactions on Neural Networks, 14(6), 1569–1572. [PubMed: 18244602]

Jan L, & Jan Y (1976). Properties of the larval neuromuscular junction in Drosophila melanogaster. Journal of Physiology, 262(1), 189–214. [PubMed: 11339]

Jan L, & Jan Y (1990). How might the diversity of potassium channels be generated? Trends in Neurosciences, 13(10), 415–419. [PubMed: 1700515]

Jan L, & Jan Y (1997). Voltage-gated and inwardly rectifying potassium channels. Journal of Physiology, 505(2), 267–282. [PubMed: 9423171]

Jones E, Oliphant T, Peterson P, et al. (2001). SciPy: open source scientific tools for Python. http://www.scipy.org/.

Kim J, Wei D, Hoffman D (2005). Kv4 potassium channel subunits control action potential repolarization and frequency-dependent broadening in rat hippocampal CA1 pyramidal neurones. Journal of Physiology, 569(1), 41–57. [PubMed: 16141270]

Levine J, & Wyman R (1973). Neurophysiology of flight in wildtype and a mutant Drosophila. PNAS, 70(4), 1050–1054. [PubMed: 4197927]

Lin W, Wright D, Muraro N, Baines R (2009). Alternative splicing in the voltage-gated sodium channel DmNav regulates activation, inactivation, and persistent current. Journal of Neurophysiology, 102(3), 1994–2006. [PubMed: 19625535]

Liss B, Franz O, Sewing S, Bruns R, Neuhoff H, Roeper J (2001). Tuning pacemaker frequency of individual dopaminergic neurons by Kv4.3L and KChip3.1 transcription. The EMBO Journal, 20(20), 5715–5724. [PubMed: 11598014]

Machin K, & Pringle J (1959). The physiology of insect fibrillar muscle. ii. mechanical properties of a beetle flight muscle. Proceedings of the Royal Society of London. Series B. Biological Sciences, 151(943), 204–225.

Mo Z, Adamson C, Davis R (2002). Dendrotoxin-sensitive k^+ currents contribute to accommodation in murine spiral ganglion neurons. The Journal of physiology, 542(3), 763–778. [PubMed: 12154177]

Murbartián J, Arias J, Perez-Reyes E, (2004). Functional impact of alternative splicing of human T-type Cav3.3 calcium channels. Journal of Neurophysiology, 92(6), 3399–3407. [PubMed: 15254077]

Nagumo J, Arimoto S, Yoshizawa S (1962). An active pulse transmission line simulating nerve axon. Proceedings of the IRE, 50(10), 2061–2070.

Neher E (1971). Two fast transient current components during voltage clamp on snail neurons. Journal of General Physiology, 58(1), 36–53. [PubMed: 5564761]

O'Donnell Olson R, Liu Z, Nomura Y, Song W, Dong K (2008). Molecular and functional characterization of voltage-gated sodium channel variants from Drosophila melanogaster. Insect Biochemistry and Molecular Biology, 38(5), 604–610. [PubMed: 18405837]

Pan Z, Selyanko A, Hadley J, Brown D, Dixon J, McKinnon D (2001). Alternative splicing of KCNQ2 potassium channel transcripts contributes to the functional diversity of M-currents. Journal of Physiology, 531(2), 347–358. [PubMed: 11230508]

Peng I-F, & Wu C-F (2007). Differential contributions of Shaker and Shab K^+ currents to neuronal firing patterns in Drosophila. Journal of Neurophysiology, 97(1), 780–794. [PubMed: 17079336]

Ping Y, Waro G, Licursi A, Smith S, Vo-Ba D, Tsunoda S (2011). Shal/Kv4 channels are required for maintaining excitability during repetitive firing and normal locomotion in Drosophila. PloS ONE, 6(1), e16043.

Pongs O, & Schwarz J (2010). Ancillary subunits associated with voltage-dependent K^+ channels. Physiological Reviews, 90(2), 755–796. [PubMed: 20393197]

Prescott S, De Koninck Y, Sejnowski T (2008). Biophysical basis for three distinct dynamical mechanisms of action potential initiation. PLoS Computational Biology, 4(10), e1000198.

Prinz A, Billimoria C, Marder E (2003). Alternative to hand-tuning conductance-based models: construction and analysis of databases of model neurons. Journal of Neurophysiology, 90(6), 3998–4015. [PubMed: 12944532]

Rinzel J (1985). Excitation dynamics: insights from simplified membrane models. Federation Proceedings, 44(15), 2944–2946. [PubMed: 2415401]

Rinzel J, & Ermentrout G (1989). Analysis of neural excitability and oscillations In Koch C & Segev I (Eds.), Methods in neuronal modelling: from synapses to networks (pp. 251–291). Cambridge, MA: MIT Press.

Ryan M, Maloney R, Reenan R, Horn R (2008). Characterization of five RNA editing sites in Shab potassium channels. Channels (Austin, Tex.), 2(3), 202–209.

Ryglewski S, & Duch C (2009). Shaker and Shal mediate transient calcium-independent potassium current in a Drosophila flight motoneuron. Journal of Neurophysiology, 102(6), 3673–3688. [PubMed: 19828724]

Ryglewski S, & Duch C (2012). Preparation of Drosophila central neurons for in situ patch clamping. Journal of Visualized Experiments, in press

Ryglewski S, Lance K, Levine R, Duch C (2012). Cav2 channels mediate low and high voltage-activated calcium currents in drosophila motoneurons. Journal of Physiology, 590(4), 809–825. [PubMed: 22183725]

Saito M, Nelson C, Salkoff L, Lingle C, (1997). A cysteine-rich domain defined by a novel exon in a Slo variant in rat adrenal chromaffin cells and PC12 cells. Journal of Biological Chemistry, 272(18), 11710–11717. [PubMed: 9115223]

Saito M, & Wu C (1991). Expression of ion channels and mutational effects in giant Drosophila neurons differentiated from cell division-arrested embryonic neuroblasts. Journal of Neuroscience, 11(7), 2135–2150. [PubMed: 1712379]

Salkoff L, Baker K, Butler A, Covarrubias M, Pak M, Wei A (1992). An essential set of K^+ channels conserved in flies, mice and humans. Trends in Neurosciences, 15(5), 161–166. [PubMed: 1377421]

Sanyal S, Narayanan R, Consoulas C, Ramiswami M (2003). Evidence for cell autonomous ap1 function in regulation of drosophila motor-neuron plasticity. BMC Neuroscience, 4, 20. [PubMed: 12969508]

Schaefer J, Worrell J, Levine R (2010). Role of intrinsic properties in Drosophila motoneuron recruitment during fictive crawling. Journal of Neurophysiology, 104(3), 1257–1266. [PubMed: 20573969]

Schilcher F.v. (1976). The behavior of cacophony, a courtship song mutant in drosophila melanogaster. Behavioral Biology, 17(2), 187–196. [PubMed: 822818]

Schulz D, Goaillard J, Marder E (2006). Variable channel expression in identified single and electrically coupled neurons in different animals. Nature Neuroscience, 9(3), 356–362. [PubMed: 16444270]

Schulz D, Goaillard J, Marder E (2007). Quantitative expression profiling of identified neurons reveals cell-specific constraints on highly variable levels of gene expression. PNAS, 104(32), 13187–13191. [PubMed: 17652510]

Schulz D, Temporal S, Barry D, Garcia M (2008). Mechanisms of voltage-gated ion channel regulation: from gene expression to localization. Cellular and Molecular Life Sciences, 65(14), 2215–2231. [PubMed: 18408887]

Shibata R, Nakahira K, Shibasaki K, Wakazono Y, Imoto K, Ikenaka K (2000). A-type K^+ current mediated by the Kv4 channel regulates the generation of action potential in developing cerebellar granule cells. Journal of Neuroscience, 20(11), 4145–4155. [PubMed: 10818150]

Sonders M, & Amara S (1996). Channels in transporters. Current Opinion in Neurobiology, 6(3), 294–302. [PubMed: 8794089]

Steriade M (2001). The intact and sliced brain. MIT Press.

Steriade M, Timofeev I, Durmuller N, Grenier F (1998). Dynamic properties of corticothalamic neurons and local cortical interneurons generating fast rhythmic (30–40 Hz) spike bursts. Journal of Neurophysiology, 79(1), 483–490. [PubMed: 9425218]

Swensen A, & Bean B (2005). Robustness of burst firing in dissociated Purkinje neurons with acute or long-term reductions in sodium conductance. Journal of Neuroscience, 25(14), 3509–3520. [PubMed: 15814781]

Tan M, Theeuwes H, Feenstra L, Borst J (2007). Membrane properties and firing patterns of inferior colliculus neurons: an in vivo patch-clamp study in rodents. Journal of neurophysiology, 98(1), 443–453. [PubMed: 17507499]

Timpe L, Jan Y, Jan L (1988). Four cdna clones from the shaker locus of drosophila induce kinetically distinct a-type potassium currents in xenopus oocytes. Neuron, 1(8), 659–667. [PubMed: 3272184]

Tobin A, Cruz-Bermúdez N, Marder E, Schulz D (2009). Correlations in ion channel mRNA in rhythmically active neurons. PLoS ONE, 4(8), e6742.

Trimmer J, & Rhodes K (2004). Localization of voltage-gated ion channels in mammalian brain. Annual Reviews of Physiology, 66, 477–519.

Tsunoda S, & Salkoff L (1995a). Genetic Analysis of Drosophila Neurons: Shal, Shaw, and Shab Encode Most Embryonic Potassium Currents. Journal of Neuroscience, 15(3), 1741–1754. [PubMed: 7891132]

Tsunoda S, & Salkoff L (1995b). The major delayed rectifier in both Drosophila neurons and muscle is encoded by Shab. Journal of Neuroscience, 15(7), 5209–5221. [PubMed: 7623146]

Watanabe I, Wang H, Sutachan J, Zhu J, Recio-Pinto E, Thornhill W (2003). Glycosylation affects rat Kv1.1 potassium channel gating by a combined surface potential and cooperative subunit interaction mechanism. Journal ofPhysiology, 550(1), 51–66.

Willms A, Baro D, Harris-Warrick R, Guckenheimer J (1999). An improved parameter estimation method for Hodgkin-Huxley models. Journal of Computational Neuroscience, 6(2), 145–168. [PubMed: 10333160]

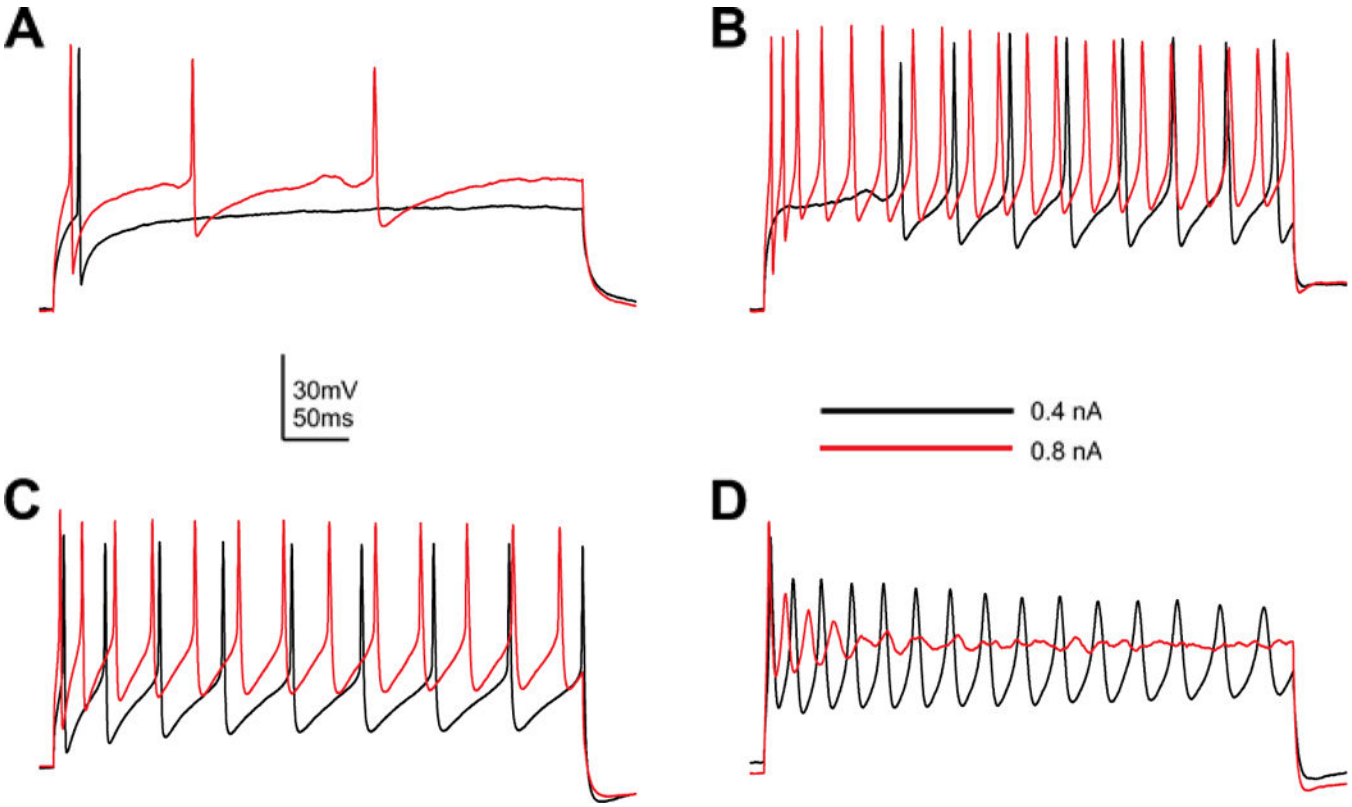

Fig. 1.

Different electrophysiological profiles recorded from *Drosophila* MN5. Intracellular recordings were made in whole-cell patch configuration from MN5 in wild-type adult *Drosophila*. At least four different firing behaviors can be observed in response to a 500 ms square-pulse current injection of 0.4 nA (*black traces*) or 0.8 nA (*red traces*). (**A**) Low-amplitude current stimulation elicits a single action potential (*black trace*), while increased stimulation elicits repetitive spiking that adapts in frequency (*red trace*). (**B**) Repetitive firing is elicited by low-amplitude stimulation, but commences only after a delay (*black trace*). Increasing the current amplitude eliminates the delay and increases the firing frequency (*red trace*). (**C**) Repetitive firing without a significant delay is induced even by low-amplitude current injection (*black trace),* while increasing the amplitude increases the firing frequency *(red trace*). (**D**) Low-amplitude stimulation produces a large initial spike, followed by triangular-shaped spikes which diminish in amplitude and broaden as stimulation continues (*black trace*). Larger stimulation amplitudes induce dampening oscillations that end in depolarization block (*red trace*)

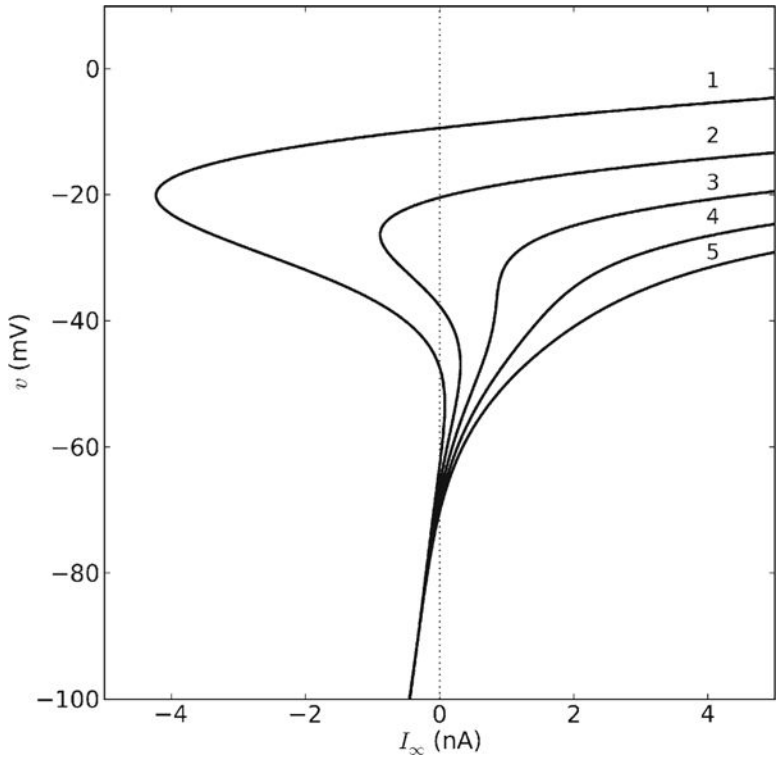

Fig. 2.

Steady-state curves resulting from variation in Shab channel expression. The steady-state current $I_\infty(\upsilon)$ was calculated according to Eq. (11) for different maximum amplitudes of the Shab current relative to the DmNa_υ current (a_K). The value of a_K was varied between 1 and 5, as indicated above the corresponding curve

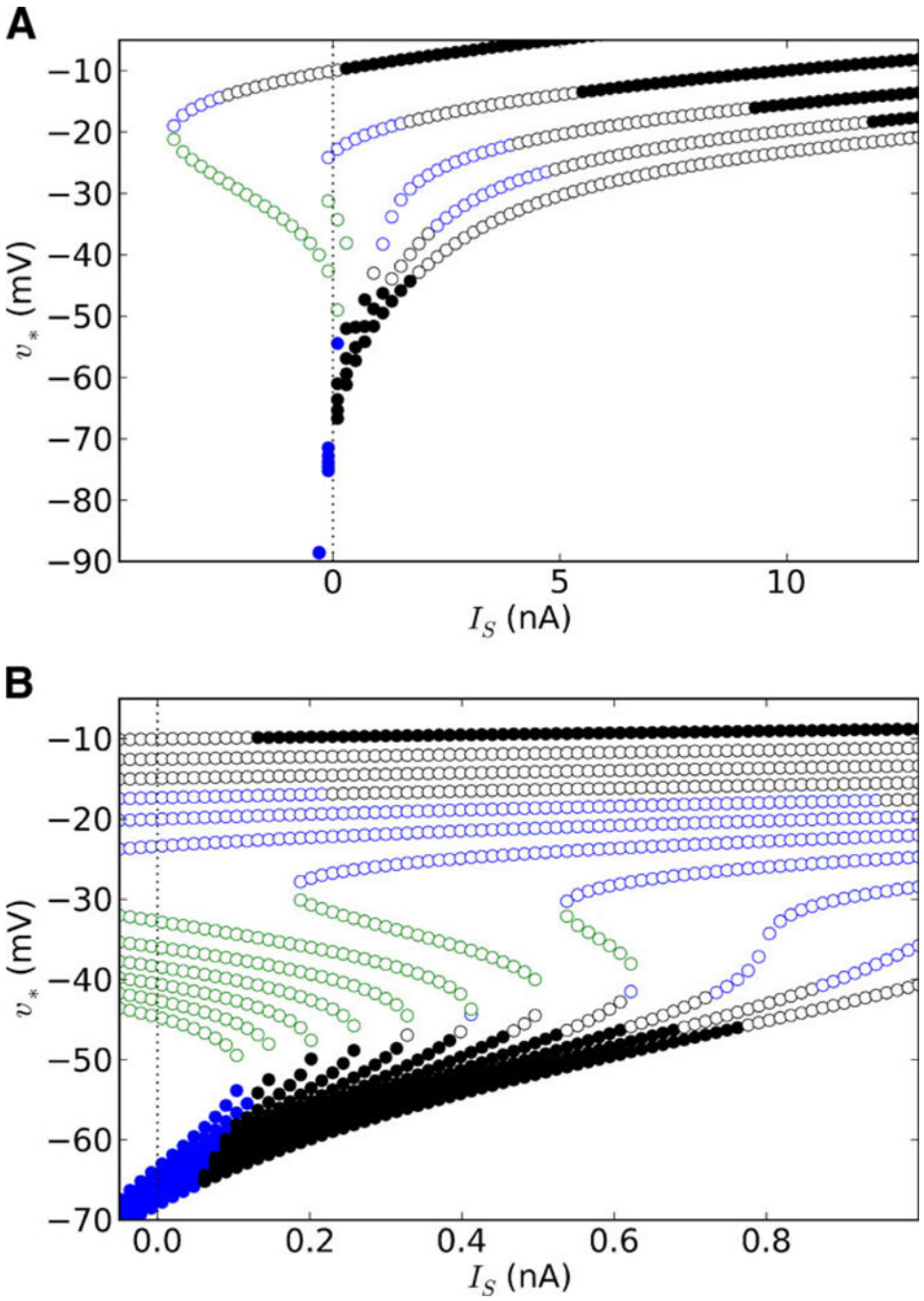

Fig. 3.

Bifurcation diagrams for different levels of Shab channel expression. *Curves* are comprised of the v-values of the fixed points (v_*) as a function of the current stimulation amplitude (Is). Note that the shapes of these curves are identical to the shapes of the $I_\infty(v)$ curves (Fig. 2), since the curve of v-values is obtained by calculating the zero crossings of $I_s - I_\infty(v)$ using different values of I_s. *Dashed line* marks where $I_s = 0$, for ease of identifying the fixed points in the absence of stimulation. Shab channel expression (a_K) was varied between 1 and 5 (as indicated) in steps of 1.0 (A), or between 1 and 3 in steps of 0.2 (B). *Open circles*

represent unstable fixed points, while *filled circles* represent asymptotically stable fixed points. *Black*, *blue*, and *green circles* represent, respectively, foci, nodes, and saddles. Parameters: $\upsilon_w = -1$, $\eta_w = 2$, $\sigma_w = 0.7$, $\bar{\tau}_w = 10$ ms

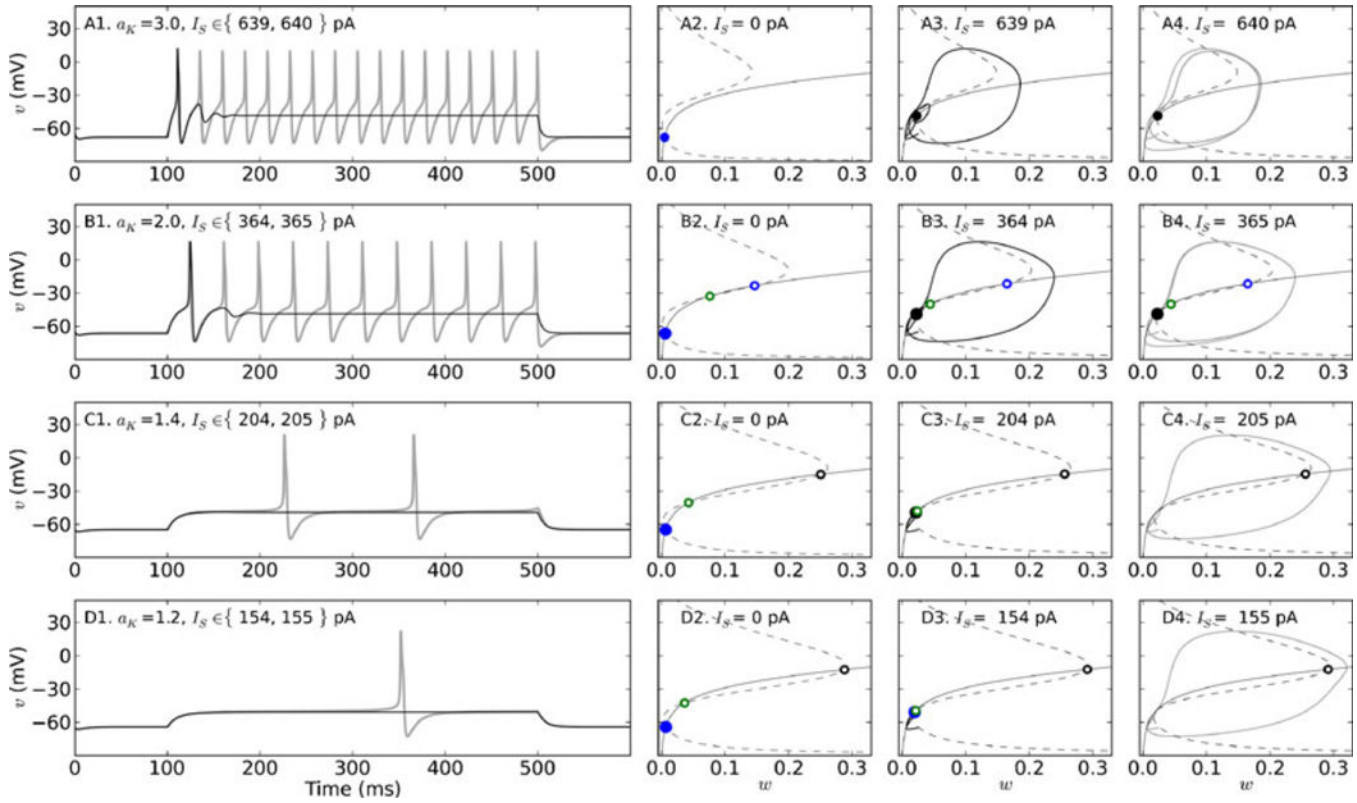

Fig. 4.

Transitions from rest to repetitive spiking for different levels of Shab channel expression. Membrane potential dynamics, nullclines, and trajectories in phase space for $a_K = 3.0$ (*A1–A4*), 2.0 (*B1–B4*), 1.4 (*C1-C4*)), or 1.2 (*D1-D4*). *A1*, *B1*, *C1*, *D1*: Responses to two 400 ms square pulses of current, the first at 1 pA below (*black traces*) and the second at I_{cyc} (*gray traces*). *A2*, *B2*, *C2*, *D2*: Nullclines I_{cyc} for v (*dashed*) and w (*solid*) are plotted in phase space in the absence of stimulation ($I_s = 0$). Intersections of the nullclines are marked with circles to indicate stable (*filled*) or unstable (*open*) fixed points. Nodes are *blue*, saddle points are *green*, and foci are *black*. If there is more the one fixed point, the one located at the lowest membrane potential has the larger marker size. *A3*, *B3*, *C3*, *D3*: Nullclines and trajectories (*solid black*) of the system in phase space corresponding to the response to current stimulation 1 pA below I_{cyc}. Nullclines and fixed points are plotted as described above. *A4*, *B4*, *C4*, *D4*: Nullclines and trajectories of the system in phase space corresponding to the response to current stimulation at I_{cyc}. Parameters: $\sigma w = 0.7$,. $\bar{\tau}_w = 10$ ms, with initial conditions $(w_0, v_0) = (0.025, -65)$. See Table 1 for all other parameters

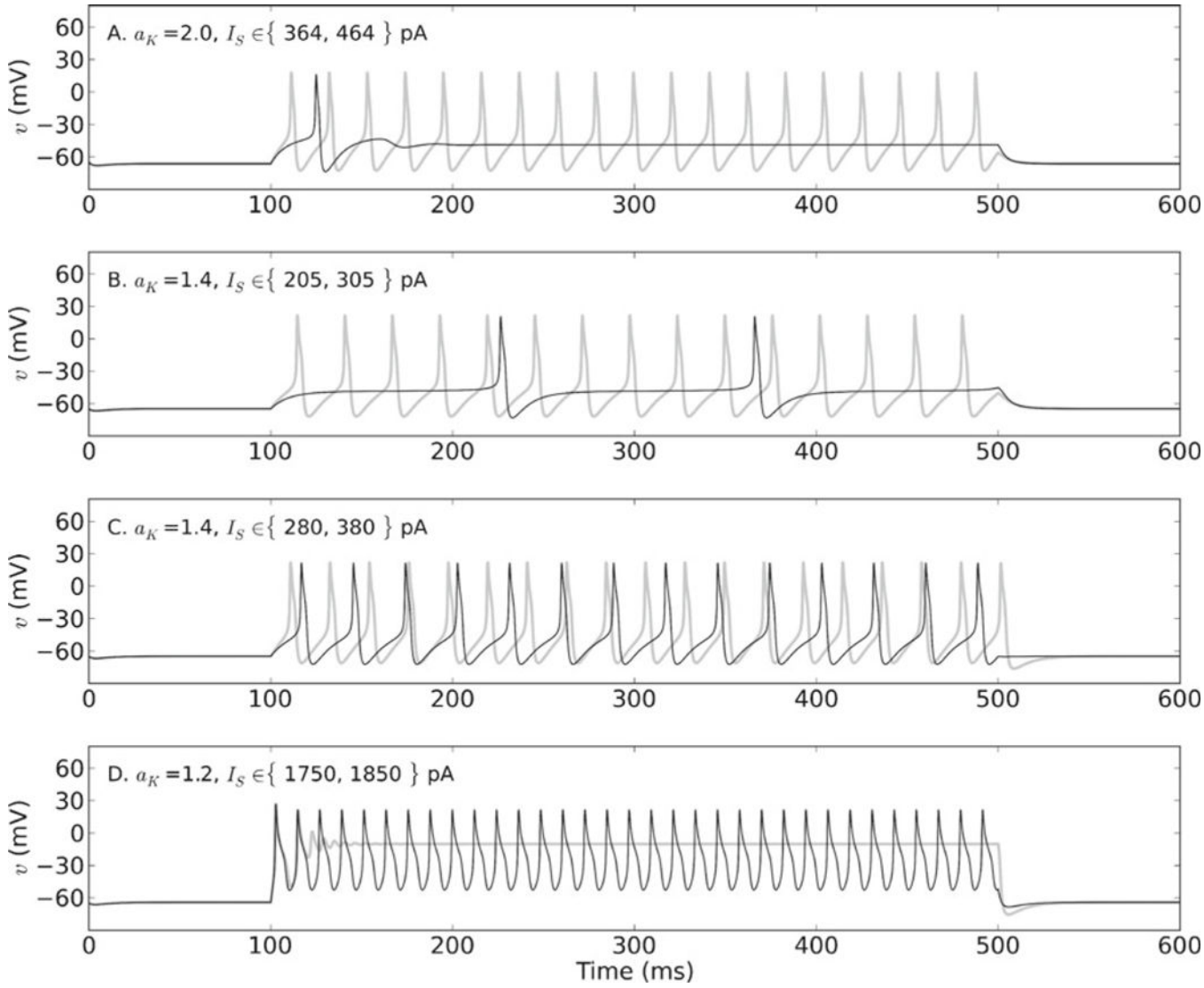

Fig. 5.

Firing behaviors produced by different combinations of Shab channel expression and stimulation amplitude. (A) Stimulating the membrane just below I_{cyc} when $a_K = 2.0$ causes a single spike followed by a depolarization that is sustained for the duration of the current pulse (*black trace*). Increasing the current amplitude by 100 pA elicits relatively high-frequency repetitive spiking (*gray trace*). Compare these responses to those of MN5 in Fig. 1(A). (B) Stimulating at I_{cyc} when $a_K = 1.4$ produces low-frequency repetitive firing with a long delay to first spike (*black trace*). Increasing the current by 100 pA abolishes the long delay and elicits higher-frequency repetitive firing (*gray trace*). Compare to MN5 recordings in Fig. 1(B). (C) Stimulating with an amplitude beyond I_{cyc} when $a_K = 1.4$ induces repetitive firing that commences shortly after stimulus onset. Increasing the current by 100 pA decreases the already short spike latency and increases the firing frequency. Compare to MN5 responses in Fig. 1(C). (D) Stimulating with a current well beyond I_{cyc} when $a_K = 1.2$ produces fast-onset repetitive spiking, but APs diminish slightly in amplitude after the first spike and have a triangular shape. Increasing the current by 100 pA produces an initial spike,

but subsequent oscillations decrease in amplitude until full depolarization block is reached. Compare to MN5 responses in Fig. 1(D). Parameters same as in Fig. 4

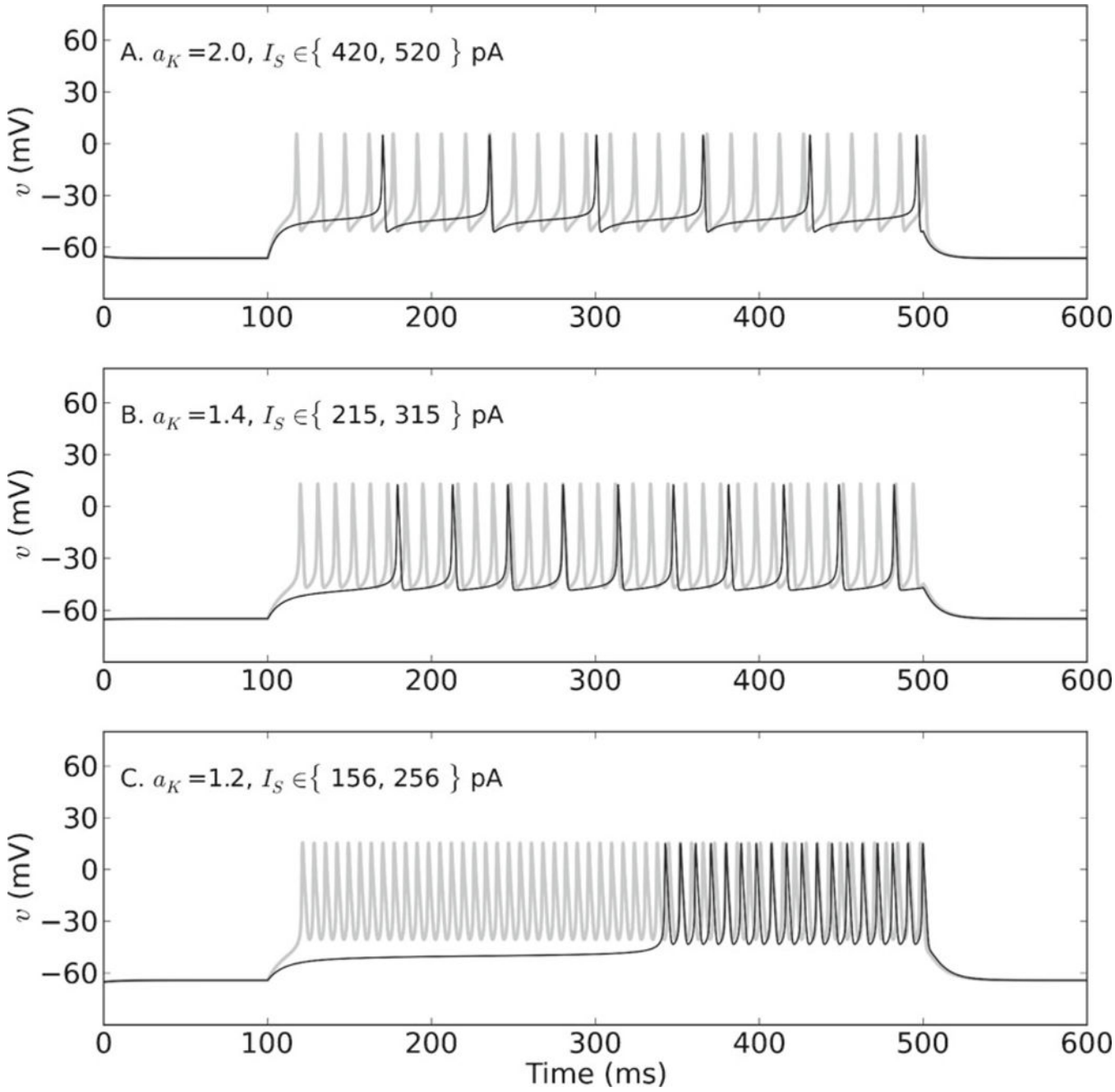

Fig. 6.

Elevated potentials and delayed firing profiles produced by variation in Shab channel activation and expression. Slower Shab channel activation results in the production of elevated potentials on which spikes ride for each a_K. Several different delayed firing profiles are also produced by varying a_K. Stimulating the membrane a little beyond I_{cyc} when a_K = 2.0 elicits repetitive spiking with a delay to first spike and a subsequent ISI of similar duration (*black trace*). Increasing the current amplitude by 100 pA decreases the spike latency and elicits higher-frequency spiking (*gray trace*). Spike shape is similar to MN5 spikes. (B) Stimulating beyond I_{cyc} when a_K = 1.4 produces a delay to first spike longer than

the subsequent ISI *(black trace*). Increasing the current by 100 pA abolishes the long delay and elicits higher-frequency repetitive firing *(gray trace*). Note similarity to delayed firing profile of MN5 in Fig. 1(B). However, spikes in this case have different concavity to those recorded from MN5. (C) Stimulating the membrane just above I_{cyc} when $a_K = 1.2$ produces a much longer delay to first spike than the ISI *(black trace*). Increasing the current amplitude eliminates the long delay and increases the firing frequency *(gray trace*). Again, this profile is similar to that in Fig. 1(B). However, the spike shape is worse than that seen when $aK = 1.4$. Parameters: $\sigma_w = 0.3$, $\bar{\tau}_w = 5$ ms

Table 1

Parameters and constants

Name	Value	Units	Description
q	$1.60217733 \times 10^{-19}$	C	Elementary charge
K	$1.38065812 \times 10^{-20}$	mJ/K	Boltzmann's constant
T	273.15 + 22	K	Absolute temperature (corresponds to room temperature at 22 °C)
$\upsilon_B = \frac{kT}{q}$	25.43	mV	Boltzmann's potential
R_{In}	100	MΩ	Input resistance
C_m	130	pF	Membrane capacitance
υ_{Na}	70	mV	Reversal potential for Na^+
υ_K	−90	mV	Reversal potential for K^+
υ_L	−60	mV	Reversal potential for leak
$\bar{a}_{\mathrm{Na}}$	13	nA	Maximal amplitude for $DmNa_\upsilon$ current
$\bar{a}_{\mathrm{K}}$	[13, 65]	nA	Maximal amplitude for Shab current
$\bar{a}_{\mathrm{L}}$	0.5	nA	Constant amplitude for leak current
$a_{Na} = \frac{\overline{a}_{Na}}{\overline{a}_{Na}}$	1		Normalized amplitude for $DmNa_\upsilon$ current
$a_K = \frac{\overline{a}_K}{\overline{a}_{Na}}$	[1,5]		Normalized amplitude for Shab current
$a_L = \frac{\overline{a}_L}{\overline{a}_{Na}}$	0.04		Normalized amplitude for leak current
$\xi = \frac{\overline{a}_{\mathrm{Na}}}{C_m}$	100	nA/nF	Scaling factor for physiologically relevant $d\upsilon/dt$
υ_m	−28	mV	Half-activation for $DmNa_\upsilon$ (Lin et al. 2009; O'Donnell Olson et al. 2008)
υ_w	−1	mV	Half-activation for Shab (Tsunoda and Salkoff 1995b)
η_m	2		Gating charge of activation for $DmNa_\upsilon$ (estimated from Lin et al. 2009)
η_w	2		Gating charge of activation for Shab (Tsunoda and Salkoff 1995b)
$\bar{\tau}_w$	5 or 10	ms	Maximum time constant for Shab (estimated from Tsunoda and Salkoff 1995b)

J Comput Neurosci. Author manuscript; available in PMC 2019 June 27.

Name	Value	Units	Description
σ_w	0.3 or 0.7		Symmetry of time constant for Shab (estimated from Tsunoda and Salkoff 1995b)

Table 2

Effects of varying aK on transition into repetitive spiking, $(\bar{\tau}_w, \sigma_w) = (10, 0.7)$

a_K	$I_\infty(v)$ curve	Bifurcation	I_{cyc} (pA)	delay (ms)	ISI (ms)
1.0	Non-monotonic	Saddle-node	112	>300	>300
1.2	Non-monotonic	Saddle-node	155	>200	>200
1.4	Non-monotonic	Saddle-node	205	>100	>100
1.6	Non-monotonic	Fold limit cycle	259	<50	<100
1.8	Non-monotonic	Fold limit cycle	312	<50	<50
2.0	Non-monotonic	Fold limit cycle	365	<25	<50
2.2	Non-monotonic	Fold limit cycle	418	<25	<50
2.4	Non-monotonic	Fold limit cycle	472	<25	<50
2.6	Monotonic	Fold limit cycle	527	<25	<50
2.8	Monotonic	Fold limit cycle	583	<25	<50
3.0	Monotonic	Fold limit cycle	640	<10	<25

J Comput Neurosci. Author manuscript; available in PMC 2019 June 27.